Stochastic motion and transcriptional dynamics of pairs of distal DNA loci on a compacted chromosome

David B Brueckner, Hongtao Chen, Lev Barinov, Benjamin Zoller, Thomas Gregor

Author: Please check editing changes carefully and respond to all queries. Inserted text is in bold blue type; deletions are in red with strike-through marks. Please mark any changes directly on the galley proofs that you receive from the printer, *not* on this document. Thank you.

Suzanne M. White, Content Production Editor, *Science*
Email: swhite@aaas.org

MOLECULAR BIOLOGY

Stochastic motion and transcriptional dynamics of pairs of distal DNA loci on a compacted chromosome

David B. Brückner[1]†, Hongtao Chen[2,3]†, Lev Barinov[3,4], Benjamin Zoller[5,6], Thomas Gregor[3,5,6]*

[1]Institute of Science and Technology, Am Campus 1, ~~3400~~ Klosterneuburg, Austria. [2]School of Life Science and Technology, ShanghaiTech University, Shanghai, China. [3]Lewis-Sigler Institute for Integrative Genomics, Princeton University, Princeton, NJ, USA. [4]Memorial Sloan Kettering Cancer Center, New York, ~~New York~~NY, USA. [5]Joseph Henry Laboratories of Physics, Princeton University, Princeton, NJ, USA. [6]Department of Developmental and Stem Cell Biology, CNRS UMR3738 Paris Cité, Institut Pasteur, Paris, France.

†These authors contributed equally to this work.
*~~To whom correspondence should be addressed~~Corresponding author. E-mail: tg2@princeton.edu.

Commented [SW1]: AU: All affiliations should be consistent either with or without postal codes. Since this was the only one that had one, I simply deleted it.

Chromosomes in the eukaryotic nucleus are highly compacted. However, for many functional processes, including transcription initiation, the pair~~-~~wise motion of distal chromosomal elements~~,~~ ~~–~~ such as enhancers and promoters~~,~~ is essential and necessitates dynamic fluidity. Here, we used a live imaging assay to simultaneously measure the positions of pairs of enhancers and promoters and their transcriptional output while systematically varying the genomic separation between these two DNA loci. Our analysis reveals the coexistence of a compact globular organization and fast subdiffusive dynamics. These combined features cause an anomalous scaling of polymer relaxation times with genomic separation leading to long-ranged correlations. Thus, encounter times of DNA loci are much less dependent on genomic distance than predicted by existing polymer models, with potential consequences for eukaryotic gene expression.

Living systems are built based on information encoded in chromosomes confined in each cell's nucleus. These meter-long DNA polymers must be highly compacted to fit into the micrometer~~n~~-sized structure (*1*, *2*). At the same time, for cells to function, chromosome organization must allow the information content to be accessed and read out through transcription (*3*, *4*). Often, transcription can only occur through the spatial interaction of DNA loci~~,~~ such as enhancers and promoters, which ~~.~~ ~~They~~ find each other dynamically and remain in physical proximity (*5*–*8*). ~~While~~ Although the distances over which many enhancers function in higher eukaryotes can be up to mega~~–~~base pairs in genomic separation (*9*–*12*), it is unknown how these elements come into proximity, what their typical distance is in three-dimensional (3D) space, and how they explore this space dynamically in the process. Specifically, it remains

unclear how the real-time physical motion of such coupled pairs of DNA loci determines transcriptional encounters and how this depends on their genomic separation.

Over the past decade, the advent of chromosome capture and imaging methods (*13*) has given key insights into the 3D spatial organization of chromosomes, with the discovery of structural features such as topologically associating domains (TADs) (*14–17*), phase-separated nuclear condensates (*18–20*), and larger-scale compartments (*21*, *22*). These organizing structures have key implications for transcriptional regulation (*23*). but they are not static. Rather, ~~However, these structures are not static but~~ they have been revealed to be heterogeneous across cells (*24*, *25*) and dynamic and short~~-~~ lived in time (*26*, *27*). The role of the real-time dynamics of pairs of loci is only beginning to be understood and remains elusive for focal contacts ~~which~~ that are key to establishing enhancer–promoter interactions in many systems (*28*).

Similarly, from a polymer physics perspective, there is a gap in our understanding of the static and dynamic properties of chromosomes. At large scales, across tens to hundreds of TADs, chromosome organization has been shown to be highly compacted in a space-filling configuration (*22*, *29*, *30*). A useful null model for this configuration is the crumpled chain (also referred to as fractal globule) with fractal dimension three (*22*, *31–33*). ~~Yet~~However, the real-time dynamics of DNA loci revealed by live-imaging experiments exhibit subdiffusion with exponents in the range of 0.5 to 0.6 ~~0.5 – 0.6~~ (*26*, *27, 34–36*), close to the predictions of the simple Rouse polymer model, which predicts a loosely packed ideal chain polymer configuration with fractal dimension two that is in contrast to~~s~~ the compacted architecture of the crumpled chain model. A promising technique to address this gap are scaling approaches that combine fractal organization and subdiffusive dynamics (*37–39*), but these have never been tested experimentally.

Thus far, experimental data~~-~~sets have given insight into ~~either~~ static organization (*14–17*, *22*, *30*, *40*), dynamic properties of chromosomes (*26*, *27, 34*, *35*, *41*), or transcription (*8*, *36*, *42–44*), but rarely all at the same time. For instance, previous live measurements of locus pairs occurred at fixed genomic separation in transcriptionally silent loci (*26*, *27*). To investigate how 3D spatial organization and dynamic locus motion control the encounter times of functional DNA loci and thus transcriptional activation, we require an approach to simultaneously monitor the movement of DNA locus pairs and transcription across a series of genomic separations in vivo.

Here, we addressed this problem by live imaging the joint dynamics of two cis-regulatory DNA elements, an enhancer, and a promoter, while monitoring the transcriptional output resulting from their functional dynamic encounters in developing fly embryos. We systematically varied~~y~~ the genomic separation between these loci spanning many TADs. Stochastic real-time trajectories of the 3D motion of the two loci showed a dynamic search process, with physical proximity required for successful transcription and a power-law scaling of transcription probability with genomic separation. ~~While~~ Although typical 3D distances between the locus pair follow a compact packing consistent with the crumpled chain model, the dynamic properties exhibit fast diffusion, albeit with a diffusion coefficient that increases with genomic separation. These features give rise to an anomalous scaling of polymer relaxation times and long-range correlations in the relative motion of the two loci. This suggests that the enhancer~~-~~ ~~–~~promoter search process is much less dependent on genomic separation than expected based on existing polymer models.

Commented [SW2]: AU: Nothing was changed in the equations and variables; I just set them inline whenever possible so that they fit better in the text. (When a paper was originally formatted in LaTeX, all numbers and variables end up in equation boxes upon conversion.) Also note that journal style is not to italicize Greek letters so this has been changed.

Commented [SW3]: AU: Just wanted to confirm that you are referring to four things here. If instead, the two cis-regulatory DNA elements ARE the enhancer and the promoter, then the punctuation should be adjusted like this: "…dynamics of two cis-regulatory DNA elements, an enhancer and a promoter, while monitoring…."

Results

Live imaging of chromosome dynamics and transcription

To simultaneously monitor the coupled motion of enhancer–promoter pairs and transcription across multiple genomic separations, we generated fly lines in which a reporter gene was introduced at various genomic locations from the well-studied *Drosophila even-skipped (eve)* locus (*8*). The locations of both the endogenous *eve* enhancers and the promoter of the reporter gene, as well as the transcriptional activity of the reporter gene, were measured together using a three-color imaging system (see the materials and methods, section 1.2, and Fig. 1A) (*8*). To facilitate transcription, the reporter cassette contained the insulator element *homie*, which allowed stable loop formation with the endogenous *homie* element in the *eve* locus (Fig. 1B).

We built seven such reporter constructs, with genomic separations s varying over close to two orders of magnitude from 58 kb to 3.3 Mb, comparable to the distances over which many enhancers function in higher eukaryotes (see the materials and methods, section 1.1) (*9*–*12*). These genomic length scales span across multiple TADs in the *Drosophila* genome, with typical median TAD sizes of ~90 kb (*45*) (here, 18 kb for the *eve* locus).

Imaging took place for ~30 min during the second half of nuclear cycle 14 (NC14) of embryo development (Fig. 1C), well after the completion of DNA replication. Sister chromatids are tightly coupled together at intervals <10 kb (*46*). Therefore, our two tagged DNA loci are connected by a single chromatin polymer composed of two coupled chromatids that were not resolved by our microscopy. Accordingly, our measurements are associated with increased localization uncertainty and reflect both intra- and inter-chromosomal interactions, which may not be fully representative of pure intra-chromosomal interactions.

Inter-locus distance scaling suggests a space-filling organization

In previous work, employing using a single fixed genomic distance (s = 149 kb) (*8*), this system was shown to exhibit three topological states, (Fig. 1C): an open configuration, O_{off}, in which O_{off} where the *homie* elements are not bound to each other, and two paired configurations, P_{off} and P_{on} P_{off} and P_{on}, where in which a loop is formed with either inactive or active transcription, respectively. Assuming that these configurations apply to all genomic distances, we determined the instantaneous topological and transcriptional states of the system. To this end, we employed used an inference approach with a hHidden Markov mModel that is based on the time series of inter-locus distances and transcriptional activity (see the materials and methods, section 2). We assigned one of these states to each measured configuration, including the hidden P_{off} P_{off} state (Fig. 1D).

A key question is how the inter-locus distances R R in the open configuration O_{off} O_{off} vary with the linear genomic separation s s. These distances exhibit broad distributions, which shift systematically with larger separation (Fig. 2A). From a polymer physics perspective, the mean distance $\langle R \rangle$ $\langle R \rangle$ is expected to scale as $s^{1/d}$ $s^{1/d}$, where d d is the fractal dimension. Whereas while an ideal chain polymer, as predicted by the simple Rouse model, has fractal

Commented [SW4]: AU: Journal style italicizes all constants and variables.

dimension $d = 2$ ~~$d = 2$~~, the compact crumpled chain organization has dimension $d = 3$ ~~$d = 3$~~ (*33*, *47*). Our experiments show a scaling exponent of $1/d = 0.31 \pm 0.07$ ~~$1/d = 0.31 \pm 0.07$~~ for genomic separations up to $s = 190$ ~~$s = 190$~~ kb, consistent with the crumpled chain model (Fig. 2B). The smaller than expected average distances observed for the largest separations ($s = 595$ kb, 3.3 Mb ~~$s = 595$kb, 3.3Mb~~) are most likely affected by the average folding of the chromosome (*48*).

The distances of the paired configurations were independent of genomic separation, as anticipated, and exhibited typical distances of 350 to 400 ~~350 – 400~~ nm (Fig. 2B), consistent with previous measurements of distances within the *eve* locus (*8*, *49*). Together, these results reveal a compact crumpled chain architecture of chromosome configurations in a range of genomic separations consistent with Hi-C experiments in *Drosophila* (*17*).

Transcriptional activity scales with genomic separation

From the latent state trajectories revealed by our inference approach, we estimated the survival curves of the transcriptionally active state (~~Fig. 2C, Methods Section~~see the materials and methods, section 2.4, and Fig. 2C). We found a median transcriptional lifetime independent of genomic separation of 10 ± 5 ~~10 ± 5~~ min (~~error: std.~~ SE across separations; Fig. 2D). This corresponds to about three to five ~~3 – 5~~ independent rounds of transcription on average, given the typical promoter switching correlation time of the system (*50*). Similarly, the relative proportion of transcriptionally active states within the paired subpopulation is insensitive to genomic separation (Fig. 2E).

Commented [SW5]: AU: Is this as meant here? (SE for "standard error" is a standard journal abbreviation that doesn't need defining.)

By ~~In~~ contrast, the overall probability of observing either of the paired configurations decreases with genomic separation~~,~~ and exhibits a power-law scaling $P(s) \sim s^{-f}$ ~~$P(s) \sim s^{-f}$~~, with $f = 0.9 \pm 0.2$ ~~$f = 0.9 \pm 0.2$~~ (Fig. 2F). ~~Since~~ Because transcriptional lifetimes are independent of distance, the scaling of $P(s)$ ~~$P(s)$~~ is likely dominated by the search of the two loci to come into contact. Different polymer models make distinct predictions of the scaling of contact probabilities (*22*, *33*, *51*). F~~:~~ for ideal chains, $f = 3/2$ ~~$f = 3/2$~~, ~~while~~ whereas crumpled chains exhibit $f \approx 1.15$ ~~$f \approx 1.15$~~ (*52*), which is close to the scaling that we observed.

To ~~test~~ determine how these results depend on the nature of the *homie* insulator ~~-~~mediated focal contacts in our system, we ~~employed~~ used a reporter construct in which the *homie* sequence was replaced by a λ ~~λ~~ DNA sequence of the same length. At a 58 ~~58~~ kb separation, transcriptional encounters still occur, albeit with a shorter median lifetime of 4.9 ± 1.2 ~~4.9 ± 1.2~~ min. Furthermore, the probability of observing a transcriptional state was reduced from $(30 \pm 5)\%$ ~~$(30 \pm 5)\%$~~ for the *homie* version to $(8.5 \pm 0.8)\%$ ~~$(8.5 \pm 0.8)\%$~~ in the no-*homie* version. By ~~In~~ contrast, ~~barely any of~~very few such encounters were found for a 149 ~~149~~ kb no-*homie* separation (*8*), where contact probability decreases from $(6 \pm 1)\%$ ~~$(6 \pm 1)\%$~~ to $>1\%$ ~~$>1\%$~~ when the *homie* sequence was replaced by a λ ~~λ~~ DNA.

Together, these results demonstrate quantitatively how both genomic sequence and genomic separation control the rate of transcriptional encounters. ~~Notably, t~~The scaling of transcription probabilities with separation suggests that the transition from the open to the paired

configuration is a key limiting step in transcriptional activation of distal DNA loci, which is limited by the time taken to diffuse into proximity.

Characterizing the subdiffusive locus search process

To understand these diffusive time scales, we considered the real-time dynamics of the blue- and green-labeled DNA loci. We found that the majority of single-cell trajectories sampled the whole range of physical distances in each topological state, ~~as~~ because they showed a similar spread as the ensemble-averaged distribution (Fig. 3, A to ~~-~~C, and fig. S8). Thus, rather than existing in constrained configurations as observed in other genomic contexts (*41*), this observation supports the picture of a dynamic search process exploring a broad range of distances.

We quantified how this search process is reflected in the motion of individual DNA loci by computing the single-locus MSD $M_1(t) = \langle (\mathbf{r}_i(t_0+t) - \mathbf{r}_i(t_0))^2 \rangle_{t_0} = \Gamma t^{\beta}$, where $\mathbf{r}_i(t)$ ~~$\mathbf{r}_i(t)$~~ is the 3D position of the locus, Γ ~~Γ~~ is ~~the~~ diffusivity, and β ~~β~~ is the dynamic exponent. This exponent quantifies how locus diffusion scales with time and can be related theoretically to the packing of the chromosome ~~via~~ through the fractal dimension d: $\beta = 2/(2+d)$ ~~d: $\beta = 2/(2+d)$~~ (*37*, *39, 53*). ~~While~~ Although the ideal chain model predicts $\beta = 1/2$ ~~$\beta = 1/2$~~ (*54*), we expected $\beta = 2/5$ ~~$\beta = 2/5$~~ for a crumpled polymer (*37*). Our system ~~shows~~ showed a scaling exponent of $\beta = 0.52 \pm 0.04$ ~~$\beta = 0.52 \pm 0.04$~~ across genomic separations (error bar: ~~std.~~ SD calculated from total variance across separations~~)~~, for both the endogenous *eve* locus (blue) and ~~for~~ the ectopic reporter (green), which is close to the prediction of the ideal chain model~~,~~ and consistent with previous works (*26*, *27, 35*) (~~Fig. 3D,E, Methods Section~~see the materials and methods, section 3, and Fig. 3, D and E). ~~Notably, o~~Our data further indicate that the single-locus dynamics are not affected by transcriptional activity, unlike previous accounts (*43*), ~~as~~ because they ~~are~~ were consistent across the three topological states (Fig. 3F).

To further understand how the locus dynamics are determined by the interplay of chromosome organization and single-locus dynamics, we analyzed the joint dynamics of the two coupled chromosomal loci. From the statistics of the 3D distance vector $\mathbf{R}(t)$ ~~$\mathbf{R}(t)$~~, we computed the two-locus MSD ~~-~~ $M_2(t) = \langle (\mathbf{R}(t_0+t) - \mathbf{R}(t_0))^2 \rangle_{t_0}$ (*26*), which quantifies the crossover between two intuitive regimes. ~~While~~ Whereas at small time ~~-~~lags, the MSD is determined by the independent diffusion of the two loci [$M_2(t) = 2\Gamma t^{\beta}$] ~~($M_2(t) = 2\Gamma t^{\beta}$)~~, it exhibits a cross~~-~~over to a plateau at large times, given by the average squared inter~~-~~locus distance [$M_2(t) = 2\langle R^2 \rangle$] ~~($M_2(t) = 2\langle R^2 \rangle$)~~ (~~Fig. 4A,B, Methods Section~~see the materials and methods, section 5, and Fig. 4, A and B). Consistent with the observed single-locus dynamics, we ~~find~~ found that the subdiffusive regime of the experimental two-locus MSD exhibited~~s~~ an exponent close to 1/2 ~~1/2~~ for those data~~-~~sets in which this regime wa~~i~~s sampled (Fig. 4A and f~~,~~ ~~F~~ig. S16). Similarly, for large time~~-~~ lags, the two-locus auto~~-~~correlation revealed~~s~~ agreement with the ideal chain scaling (Fig. 4, C and ~~,~~D). Thus, the full time ~~-~~dependence of the MSD is well described by the ideal chain predictions, both for single and coupled loci.

Inter-locus relaxation times exhibit an anomalous scaling with genomic separation

Having established the static and dynamic properties of the system, we ~~now ask~~next investigated ~~about~~ the consequences of these features for the time scales of the two-locus search process.

This process is determined by the interplay of chromosome dynamics and organization and can be characterized by a relaxation time τ ~~τ~~, which corresponds to the time scale of the crossover of the two regimes of the two-locus MSD (Fig. 2A). Specifically, τ ~~τ~~ is the time taken by the two loci to diffuse (dynamics) over their typical distance of separation (organization): $\Gamma\tau^{\beta} \sim s^{2/d}$ ~~$\Gamma\tau^{\beta} \sim s^{2/d}$~~. This relationship predicts a scaling of relaxation times with genomic separation $\tau \sim s^{\gamma}$ ~~$\tau \sim s^{\gamma}$~~. ~~F~~For ideal chains with fractal dimension $d = 2$ ~~$d = 2$~~ and a diffusion exponent $\beta = 1/2$ ~~$\beta = 1/2$~~, this yields the classical result $\gamma = 2$ ~~$\gamma = 2$~~. By ~~In~~ contrast, for crumpled chains, $\beta = 2/5$ ~~$\beta = 2/5$~~ and $d = 3$ ~~$d = 3$~~, yielding $\gamma = 5/3$ ~~$\gamma = 5/3$~~ (see the ~~Methods Section~~materials and methods, section 5, and t~~T~~able S7).

To infer the relaxation time in our data as a function of genomic separation, we performed a Bayesian fitting of the two-locus MSD with the ideal chain expression (*26*) (see the ~~Methods Section~~materials and methods, section 4.1). We found that the fitted two-locus diffusion coefficient increased~~s~~ with genomic separation up to 595 ~~595~~ kb, with an approximate scaling $\Gamma(s) \sim s^{0.27 \pm 0.03}$ ~~$\Gamma(s) \sim s^{0.27 \pm 0.03}$~~ (Fig. 4E). This scaling appeared~~s~~ to plateau for the largest genomic separation (3.3 ~~3.3~~ Mb) at a value close to the single locus diffusion, which remained~~s~~ approximately constant across separations (Fig. 4E). ~~Notably, t~~The absolute value of the diffusivity at the plateau wa~~i~~s almost 20-fold larger than previous measurements in mammalian stem cells with similar genomic separation (*26*), suggesting comparatively fast chromosome dynamics (~~Fig~~fig. S23).

The relaxation time wa~~i~~s determined by combining our estimate of the two-locus diffusivity with the average inter~~-~~locus distances. The combination of static and dynamic exponents in our system, as well as the scale-dependent diffusivity, results in an anomalous scaling of relaxation times with genomic separation with an exponent $\gamma = 0.7 \pm 0.2$ ~~$\gamma = 0.7 \pm 0.2$~~ (Fig. 4F). This exponent corresponds to a much shallower scaling with separation than predicted by either the ideal or crumpled chain theory. This result wa~~i~~s further confirmed by a data collapse of the two-locus auto~~-~~correlation functions (Fig. 4D and f~~, F~~ig. S20). Although ~~While~~ these results are derived from the trajectories in the O_{off} ~~O_{off}~~ state, they are insensitive to the details of the state inference (f~~F~~ig. S11). In sum, the key result here is that the relaxation time, which sets the time scale of two-locus encounters, is much less dependent on genomic separation than predicted by existing polymer models.

Anomalous relaxation time scaling induces long-ranged velocity correlations

The anomalous relaxation time scaling makes a key prediction for the correlations of the absolute motion of DNA loci, quantified by the velocity cross-correlation $C_{vv}^{(\delta)}(t) = \langle \mathbf{v}_i^{(\delta)}(t_0) \cdot \mathbf{v}_j^{(\delta)}(t_0 + t) \rangle_{t_0}$. These correlations are determined by the relaxation time through the dimensionless ratio δ/τ ~~δ / τ~~, where δ ~~δ~~ is the experimental observation time ~~-~~scale (Fig. 4G) (*55*). Having determined the relaxation times τ ~~τ~~, one can therefore make a parameter-free prediction of the correlations, which decay substantially more slowly than for the ideal Rouse model (~~Fig. 4H, green and grey lines, Methods Section~~see the materials and methods, section 4.3, and Fig. 4H, green and gray lines). ~~Notably, W~~~~w~~e found that the experimental correlations we~~a~~re quantitatively captured by this parameter-free prediction (Fig. 4H), including the full time ~~-~~dependence of the correlations (f~~F~~ig. S22). This demonstrates that the anomalous

relaxation time scaling indeed leads to long-ranged velocity cross-correlations of chromosomal loci, pointing toward potential long-range interactions.

Discussion

We developed an experimental approach to perform in vivo imaging of the joint dynamics of enhancer–promoter pairs with varying genomic separation and simultaneous monitoring of their transcriptional output. Observing the dynamics of pairs of DNA loci has only become possible recently and has been done for tagged DNA loci at a single fixed genomic separation (*8*, *26*, *27, 36*). Here, we show how imaging across genomic separations gives insight into the relative motion, dynamic encounters, and transcriptional activation of such loci.

Many features of the two-locus dynamics, including the subdiffusive exponent close to 0.5 0.5, are very well conserved with measurements of CTCF sites at TAD boundaries in mammalian systems (*26*, *27*), despite CTCF not being essential for *Drosophila* embryogenesis (*56*). In absolute numbers, however, our measurements revealed large diffusion coefficients of DNA loci that are, around ~20-fold larger than in mammalian cells (*26*) (fFig. S23). Early fly development follows a tight schedule, suggesting that the chromosome dynamics may have evolved to operate on much faster time scales than mammalian systems. ByIn contrast, the median lifetime of focal contacts in our system of 12 ± 5 12 ± 5 min is well within the range of typical CTCF loop lifetimes of 10 to 30 10 – 30 min in mammalian cells (*26*, *27*). These time scales facilitate transcriptional lifetimes of 10 ± 5 10 ± 5 min in our system, which in the absence of the *homie* insulator are reduced to 4.9 ± 1.2 4.9 ± 1.2 min, highlighting the importance of focal elements for contact formation in *Drosophila*.

To initiate such transcriptional encounters, the two loci perform a search process to reach physical proximity. The time scale of this search process is given by the lifetimes of the unpaired O_{off} O_{off} state, which depends on multiple factors. These factors typically include the landscape of the search process (*57*, *58*), the biochemical binding properties of the focal elements when proximity has been reached (*59*), and the correlation time of the system (, i.e., the relaxation time). Indeed, we find found that lifetimes increased with the relaxation times, and are were approximately ~10 10 times larger on average (fFig. S19).

We have demonstrated how key features of our system, —tight crumpled chain packing, subdiffusion with exponent 0.5, and a separation-dependent two-locus diffusivity, —lead to relaxation times that are much less dependent on genomic separation than predicted by existing polymer models. Indeed, for an ideal Rouse polymer, the relaxation time for our largest genomic separation (3.3 3.3 Mb) would be ~3000 ~3000 times longer than for the shortest 58- 58 kb separation. Our measurements, however, revealed that it only takes ~20 ~20 times longer, corresponding to a more than >100-fold reduction. This reduced dependence on distance implies that transcriptional encounters are possible across large genomic distances, allowing enhancers dispersed across the chromosome to find their target promoter efficiently. This might be one of the reasons why that evolution can act on distal sequences from a given target promoter. Overall, our findings have crucial implications for the spatiotemporal organization of the cell nucleus, including the dynamics of long-range focal contacts (*28*) and mammalian enhancer-promoter interactions (*9–12*, *44*).

From a polymer physics perspective, our measured exponents suggest that the relationship between static and dynamic properties in the generalized Rouse framework, which relies on the assumption of local friction, does not apply to chromosomes. This ~~suggests~~ implies that long-range interactions~~,~~ such as hydrodynamics or active motor-mediated interactions (*60*, *61*) could play a role. Indeed, the simplest polymer model that relaxes the Rouse assumption and includes long-range hydrodynamic interactions, the Zimm model (*54*), predicts a scaling relationship of relaxation times with genomic separations with an exponent of $\gamma = 1$ ~~$\gamma = 1$~~ (t~~T~~able S7), which is close to our measured value of $\gamma \approx 0.7$ ~~$\gamma \approx 0.7$~~. Furthermore, the observed separation-dependent diffusivity points to additional interactions or heterogeneities along the polymer. Such heterogeneities could be ~~due to~~caused by a number of processes, such as cross-linking (*41*), out-of-equilibrium activity (*61*), entanglements (*62*), or the presence of condensates (*18–20*). Together, these processes may orchestrate the anomalous scaling of relaxation times with genomic separation. In future work, the mechanistic underpinnings of our findings should be tested ~~through~~ using polymer simulations (*40*, *41*, *51*, *63–69*) to generate hypotheses for new sets of experiments.

References and Notes

1. W. Flemming. *Zellsubstanz, Kern Und Zelltheilung* (Vogel, 1882).
2. R. Milo, R. Phillips, *Cell Biology by the Numbers* (CRC Press, 2015).
3. R. Stadhouders, G. J. Filion, T. Graf, Transcription factors and 3D genome conformation in cell-fate decisions. *Nature* **569**, 345–354 (2019). doi:10.1038/s41586-019-1182-7 Medline
4. B. van Steensel, E. E. M. Furlong, The role of transcription in shaping the spatial organization of the genome. *Nat. Rev. Mol. Cell Biol.* **20**, 327–337 (2019). doi:10.1038/s41580-019-0114-6 Medline
5. M. Levine, Transcriptional enhancers in animal development and evolution. *Curr. Biol.* **20**, R754–R763 (2010). doi:10.1016/j.cub.2010.06.070 Medline
6. T. K. Kim, R. Shiekhattar, Architectural and functional commonalities between enhancers and promoters. *Cell* **162**, 948–959 (2015). doi:10.1016/j.cell.2015.08.008 Medline
7. D. Vernimmen, W. A. Bickmore, The hierarchy of transcriptional activation: From enhancer to promoter. *Trends Genet.* **31**, 696–708 (2015). doi:10.1016/j.tig.2015.10.004 Medline
8. H. Chen, M. Levo, L. Barinov, M. Fujioka, J. B. Jaynes, T. Gregor, Dynamic interplay between enhancer-promoter topology and gene activity. *Nat. Genet.* **50**, 1296–1303 (2018). doi:10.1038/s41588-018-0175-z Medline
9. B. Tolhuis, R. J. Palstra, E. Splinter, F. Grosveld, W. de Laat, Looping and interaction between hypersensitive sites in the active β-globin locus. *Mol. Cell* **10**, 1453–1465 (2002). doi:10.1016/S1097-2765(02)00781-5 Medline
10. V. V. Uslu, M. Petretich, S. Ruf, K. Langenfeld, N. A. Fonseca, J. C. Marioni, F. Spitz, Long-range enhancers regulating Myc expression are required for normal facial morphogenesis. *Nat. Genet.* **46**, 753–758 (2014). doi:10.1038/ng.2971 Medline

11. Y. Zhang, C. H. Wong, R. Y. Birnbaum, G. Li, R. Favaro, C. Y. Ngan, J. Lim, E. Tai, H. M. Poh, E. Wong, F. H. Mulawadi, W. K. Sung, S. Nicolis, N. Ahituv, Y. Ruan, C. L. Wei, Chromatin connectivity maps reveal dynamic promoter-enhancer long-range associations. *Nature* **504**, 306–310 (2013). doi:10.1038/nature12716 Medline

12. A. Sanyal, B. R. Lajoie, G. Jain, J. Dekker, The long-range interaction landscape of gene promoters. *Nature* **489**, 109–113 (2012). doi:10.1038/nature11279 Medline

13. Y. Huang, R. Neijts, W. de Laat, How chromosome topologies get their shape: Views from proximity ligation and microscopy methods. *FEBS Lett.* **594**, 3439–3449 (2020). doi:10.1002/1873-3468.13961 Medline

14. J. R. Dixon, S. Selvaraj, F. Yue, A. Kim, Y. Li, Y. Shen, M. Hu, J. S. Liu, B. Ren, Topological domains in mammalian genomes identified by analysis of chromatin interactions. *Nature* **485**, 376–380 (2012). doi:10.1038/nature11082 Medline

15. C. Hou, L. Li, Z. S. Qin, V. G. Corces, Gene density, transcription, and insulators contribute to the partition of the *Drosophila* genome into physical domains. *Mol. Cell* **48**, 471–484 (2012). doi:10.1016/j.molcel.2012.08.031 Medline

16. E. P. Nora, B. R. Lajoie, E. G. Schulz, L. Giorgetti, I. Okamoto, N. Servant, T. Piolot, N. L. van Berkum, J. Meisig, J. Sedat, J. Gribnau, E. Barillot, N. Blüthgen, J. Dekker, E. Heard, Spatial partitioning of the regulatory landscape of the X-inactivation centre. *Nature* **485**, 381–385 (2012). doi:10.1038/nature11049 Medline

17. T. Sexton, E. Yaffe, E. Kenigsberg, F. Bantignies, B. Leblanc, M. Hoichman, H. Parrinello, A. Tanay, G. Cavalli, Three-dimensional folding and functional organization principles of the *Drosophila* genome. *Cell* **148**, 458–472 (2012). doi:10.1016/j.cell.2012.01.010 Medline

18. A. Boija, I. A. Klein, B. R. Sabari, A. Dall'Agnese, E. L. Coffey, A. V. Zamudio, C. H. Li, K. Shrinivas, J. C. Manteiga, N. M. Hannett, B. J. Abraham, L. K. Afeyan, Y. E. Guo, J. K. Rimel, C. B. Fant, J. Schuijers, T. I. Lee, D. J. Taatjes, R. A. Young, Transcription Factors Activate Genes through the Phase-Separation Capacity of Their Activation Domains. *Cell* **175**, 1842–1855.e16 (2018). doi:10.1016/j.cell.2018.10.042 Medline

19. W.-K. Cho, J.-H. Spille, M. Hecht, C. Lee, C. Li, V. Grube, I. I. Cisse, Mediator and RNA polymerase II clusters associate in transcription-dependent condensates. *Science* **361**, 412–415 (2018). doi:10.1126/science.aar4199 Medline

20. M. Conte, E. Irani, A. M. Chiariello, A. Abraham, S. Bianco, A. Esposito, M. Nicodemi, Loop-extrusion and polymer phase-separation can co-exist at the single-molecule level to shape chromatin folding. *Nat. Commun.* **13**, 4070 (2022). doi:10.1038/s41467-022-31856-6 Medline

21. C. S. Osborne, L. Chakalova, K. E. Brown, D. Carter, A. Horton, E. Debrand, B. Goyenechea, J. A. Mitchell, S. Lopes, W. Reik, P. Fraser, Active genes dynamically colocalize to shared sites of ongoing transcription. *Nat. Genet.* **36**, 1065–1071 (2004). doi:10.1038/ng1423 Medline

22. E. Lieberman-Aiden, N. L. van Berkum, L. Williams, M. Imakaev, T. Ragoczy, A. Telling, I. Amit, B. R. Lajoie, P. J. Sabo, M. O. Dorschner, R. Sandstrom, B. Bernstein, M. A. Bender, M. Groudine, A. Gnirke, J. Stamatoyannopoulos, L. A. Mirny, E. S. Lander, J.

Dekker, Comprehensive mapping of long-range interactions reveals folding principles of the human genome. *Science* **326**, 289–293 (2009). doi:10.1126/science.1181369 Medline

23. O. Symmons, V. V. Uslu, T. Tsujimura, S. Ruf, S. Nassari, W. Schwarzer, L. Ettwiller, F. Spitz, Functional and topological characteristics of mammalian regulatory domains. *Genome Res.* **24**, 390–400 (2014). doi:10.1101/gr.163519.113 Medline

24. T. J. Stevens, D. Lando, S. Basu, L. P. Atkinson, Y. Cao, S. F. Lee, M. Leeb, K. J. Wohlfahrt, W. Boucher, A. O'Shaughnessy-Kirwan, J. Cramard, A. J. Faure, M. Ralser, E. Blanco, L. Morey, M. Sansó, M. G. S. Palayret, B. Lehner, L. Di Croce, A. Wutz, B. Hendrich, D. Klenerman, E. D. Laue, 3D structures of individual mammalian genomes studied by single-cell Hi-C. *Nature* **544**, 59–64 (2017). doi:10.1038/nature21429 Medline

25. M. V. Arrastia, J. W. Jachowicz, N. Ollikainen, M. S. Curtis, C. Lai, S. A. Quinodoz, D. A. Selck, R. F. Ismagilov, M. Guttman, Single-cell measurement of higher-order 3D genome organization with scSPRITE. *Nat. Biotechnol.* **40**, 64–73 (2022). doi:10.1038/s41587-021-00998-1 Medline

26. M. Gabriele, H. B. Brandão, S. Grosse-Holz, A. Jha, G. M. Dailey, C. Cattoglio, T. S. Hsieh, L. Mirny, C. Zechner, A. S. Hansen, Dynamics of CTCF- and cohesin-mediated chromatin looping revealed by live-cell imaging. *Science* **376**, 496–501 (2022). doi:10.1126/science.abn6583 Medline

27. P. Mach, P. I. Kos, Y. Zhan, J. Cramard, S. Gaudin, J. Tünnermann, E. Marchi, J. Eglinger, J. Zuin, M. Kryzhanovska, S. Smallwood, L. Gelman, G. Roth, E. P. Nora, G. Tiana, L. Giorgetti, Cohesin and CTCF control the dynamics of chromosome folding. *Nat. Genet.* **54**, 1907–1918 (2022). doi:10.1038/s41588-022-01232-7 Medline

28. M. Levo, J. Raimundo, X. Y. Bing, Z. Sisco, P. J. Batut, S. Ryabichko, T. Gregor, M. S. Levine, Transcriptional coupling of distant regulatory genes in living embryos. *Nature* **605**, 754–760 (2022). doi:10.1038/s41586-022-04680-7 Medline

29. S. Wang, J.-H. Su, B. J. Beliveau, B. Bintu, J. R. Moffitt, C. T. Wu, X. Zhuang, Spatial organization of chromatin domains and compartments in single chromosomes. *Science* **353**, 598–602 (2016). doi:10.1126/science.aaf8084 Medline

30. B. Bintu, L. J. Mateo, J. H. Su, N. A. Sinnott-Armstrong, M. Parker, S. Kinrot, K. Yamaya, A. N. Boettiger, X. Zhuang, Super-resolution chromatin tracing reveals domains and cooperative interactions in single cells. *Science* **362**, eaau1783 (2018). doi:10.1126/science.aau1783 Medline

31. A. Grosberg, Y. Rabin, S. Havlin, A. Neer, Crumpled globule model of the three-dimensional structure of DNA. *Europhys. Lett.* **23**, 373–378 (1993). doi:10.1209/0295-5075/23/5/012

32. A. Yu. Grosberg, S. K. Nechaev, E. I. Shakhnovich, The role of topological constraints in the kinetics of collapse of macromolecules. *J. Phys. (Paris)* **49**, 2095–2100 (1988). doi:10.1051/jphys:0198800490120209500

33. L. A. Mirny, The fractal globule as a model of chromatin architecture in the cell. *Chromosome Res.* **19**, 37–51 (2011). doi:10.1007/s10577-010-9177-0 Medline

34. S. C. Weber, A. J. Spakowitz, J. A. Theriot, Bacterial chromosomal loci move subdiffusively through a viscoelastic cytoplasm. *Phys. Rev. Lett.* **104**, 238102 (2010). doi:10.1103/PhysRevLett.104.238102 Medline

35. J. S. Lucas, Y. Zhang, O. K. Dudko, C. Murre, 3D trajectories adopted by coding and regulatory DNA elements: First-passage times for genomic interactions. *Cell* **158**, 339–352 (2014). doi:10.1016/j.cell.2014.05.036 Medline

36. J. M. Alexander, J. Guan, B. Li, L. Maliskova, M. Song, Y. Shen, B. Huang, S. Lomvardas, O. D. Weiner, Live-cell imaging reveals enhancer-dependent *Sox2* transcription in the absence of enhancer proximity. *eLife* **8**, e41769 (2019). doi:10.7554/eLife.41769 Medline

37. M. V. Tamm, L. I. Nazarov, A. A. Gavrilov, A. V. Chertovich, Anomalous diffusion in fractal globules. *Phys. Rev. Lett.* **114**, 178102 (2015). doi:10.1103/PhysRevLett.114.178102 Medline

38. S. Shinkai, T. Nozaki, K. Maeshima, Y. Togashi, Dynamic nucleosome movement provides structural information of topological chromatin domains in living human cells. *PLOS Comput. Biol.* **12**, e1005136 (2016). doi:10.1371/journal.pcbi.1005136 Medline

39. K. E. Polovnikov, M. Gherardi, M. Cosentino-Lagomarsino, M. V. Tamm, Fractal folding and medium viscoelasticity contribute jointly to chromosome dynamics. *Phys. Rev. Lett.* **120**, 088101 (2018). doi:10.1103/PhysRevLett.120.088101 Medline

40. M. Nicodemi, A. Pombo, Models of chromosome structure. *Curr. Opin. Cell Biol.* **28**, 90–95 (2014). doi:10.1016/j.ceb.2014.04.004 Medline

41. N. Khanna, Y. Zhang, J. S. Lucas, O. K. Dudko, C. Murre, Chromosome dynamics near the sol-gel phase transition dictate the timing of remote genomic interactions. *Nat. Commun.* **10**, 2771 (2019). doi:10.1038/s41467-019-10628-9 Medline

42. T. Germier, S. Kocanova, N. Walther, A. Bancaud, H. A. Shaban, H. Sellou, A. Z. Politi, J. Ellenberg, F. Gallardo, K. Bystricky, Real-time imaging of a single gene reveals transcription-initiated local confinement. *Biophys. J.* **113**, 1383–1394 (2017). doi:10.1016/j.bpj.2017.08.014 Medline

43. B. Gu, T. Swigut, A. Spencley, M. R. Bauer, M. Chung, T. Meyer, J. Wysocka, Transcription-coupled changes in nuclear mobility of mammalian cis-regulatory elements. *Science* **359**, 1050–1055 (2018). doi:10.1126/science.aao3136 Medline

44. J. Zuin, G. Roth, Y. Zhan, J. Cramard, J. Redolfi, E. Piskadlo, P. Mach, M. Kryzhanovska, G. Tihanyi, H. Kohler, M. Eder, C. Leemans, B. van Steensel, P. Meister, S. Smallwood, L. Giorgetti, Nonlinear control of transcription through enhancer-promoter interactions. *Nature* **604**, 571–577 (2022). doi:10.1038/s41586-022-04570-y Medline

45. S. V. Ulianov, V. V. Zakharova, A. A. Galitsyna, P. I. Kos, K. E. Polovnikov, I. M. Flyamer, E. A. Mikhaleva, E. E. Khrameeva, D. Germini, M. D. Logacheva, A. A. Gavrilov, A. S. Gorsky, S. K. Nechaev, M. S. Gelfand, Y. S. Vassetzky, A. V. Chertovich, Y. Y. Shevelyov, S. V. Razin, Order and stochasticity in the folding of individual *Drosophila* genomes. *Nat. Commun.* **12**, 41 (2021). doi:10.1038/s41467-020-20292-z Medline

46. B. L. Hua, T. L. Orr-Weaver, DNA replication control during *Drosophila* development: Insights into the onset of S phase, replication initiation, and fork progression. *Genetics* **207**, 29–47 (2017). doi:10.1534/genetics.115.186627 Medline

47. B. Avşaroğlu, G. Bronk, S. Gordon-Messer, J. Ham, D. A. Bressan, J. E. Haber, J. Kondev, Effect of chromosome tethering on nuclear organization in yeast. *PLOS ONE* **9**, e102474 (2014). doi:10.1371/journal.pone.0102474 Medline

48. J. Dekker, M. A. Marti-Renom, L. A. Mirny, Exploring the three-dimensional organization of genomes: Interpreting chromatin interaction data. *Nat. Rev. Genet.* **14**, 390–403 (2013). doi:10.1038/nrg3454 Medline

49. L. Barinov, S. Ryabichko, W. Bialek, T. Gregor, Transcription-dependent spatial organization of a gene locus. arXiv:2012.15819 [q-bio.MN] (2020).

50. B. Zoller, S. C. Little, T. Gregor, Diverse spatial expression patterns emerge from unified kinetics of transcriptional bursting. *Cell* **175**, 835–847.e25 (2018). doi:10.1016/j.cell.2018.09.056 Medline

51. A. Rosa, N. B. Becker, R. Everaers, Looping probabilities in model interphase chromosomes. *Biophys. J.* **98**, 2410–2419 (2010). doi:10.1016/j.bpj.2010.01.054 Medline

52. J. D. Halverson, W. B. Lee, G. S. Grest, A. Y. Grosberg, K. Kremer, Molecular dynamics simulation study of nonconcatenated ring polymers in a melt. I. Statics. *J. Chem. Phys.* **134**, 204904 (2011). doi:10.1063/1.3587137 Medline

53. P. G. De Gennes, Dynamics of entangled polymer solutions. I. The Rouse Model. *Macromolecules* **9**, 587–593 (1976). doi:10.1021/ma60052a011

54. M. Rubinstein, R. H. Colby, *Polymer Physics* (Oxford Univ. Press, 2003).

55. T. J. Lampo, A. S. Kennard, A. J. Spakowitz, Physical modeling of dynamic coupling between chromosomal loci. *Biophys. J.* **110**, 338–347 (2016). doi:10.1016/j.bpj.2015.11.3520 Medline

56. A. Kaushal, G. Mohana, J. Dorier, I. Özdemir, A. Omer, P. Cousin, A. Semenova, M. Taschner, O. Dergai, F. Marzetta, C. Iseli, Y. Eliaz, D. Weisz, M. S. Shamim, N. Guex, E. Lieberman Aiden, M. C. Gambetta, CTCF loss has limited effects on global genome architecture in *Drosophila* despite critical regulatory functions. *Nat. Commun.* **12**, 1011 (2021). doi:10.1038/s41467-021-21366-2 Medline

57. G. Wilemski, M. Fixman, Diffusion-controlled intrachain reactions of polymers. I Theory. *J. Chem. Phys.* **60**, 866–877 (1974). doi:10.1063/1.1681162

58. A. Szabo, K. Schulten, Z. Schulten, First passage time approach to diffusion controlled reactions. *J. Chem. Phys.* **72**, 4350–4357 (1980). doi:10.1063/1.439715

59. M. Fujioka, H. Mistry, P. Schedl, J. B. Jaynes, Determinants of chromosome architecture: Insulator pairing in cis and in trans. *PLOS Genet.* **12**, e1005889 (2016). doi:10.1371/journal.pgen.1005889 Medline

60. R. Bruinsma, A. Y. Grosberg, Y. Rabin, A. Zidovska, Chromatin hydrodynamics. *Biophys. J.* **106**, 1871–1881 (2014). doi:10.1016/j.bpj.2014.03.038 Medline

61. M. M. Tortora, H. Salari, D. Jost, Chromosome dynamics during interphase: A biophysical perspective. *Curr. Opin. Genet. Dev.* **61**, 37–43 (2020). doi:10.1016/j.gde.2020.03.001 Medline

62. R. Kawamura, L. H. Pope, M. O. Christensen, M. Sun, K. Terekhova, F. Boege, C. Mielke, A. H. Andersen, J. F. Marko, Mitotic chromosomes are constrained by topoisomerase II-sensitive DNA entanglements. *J. Cell Biol.* **188**, 653–663 (2010). doi:10.1083/jcb.200910085 Medline

63. A. Rosa, R. Everaers, Structure and dynamics of interphase chromosomes. *PLOS Comput. Biol.* **4**, e1000153 (2008). doi:10.1371/journal.pcbi.1000153 Medline

64. M. Barbieri, M. Chotalia, J. Fraser, L.-M. Lavitas, J. Dostie, A. Pombo, M. Nicodemi, Complexity of chromatin folding is captured by the strings and binders switch model. *Proc. Natl. Acad. Sci. U.S.A.* **109**, 16173–16178 (2012). doi:10.1073/pnas.1204799109 Medline

65. L. Giorgetti, R. Galupa, E. P. Nora, T. Piolot, F. Lam, J. Dekker, G. Tiana, E. Heard, Predictive polymer modeling reveals coupled fluctuations in chromosome conformation and transcription. *Cell* **157**, 950–963 (2014). doi:10.1016/j.cell.2014.03.025 Medline

66. L. Liu, G. Shi, D. Thirumalai, C. Hyeon, Chain organization of human interphase chromosome determines the spatiotemporal dynamics of chromatin loci. *PLOS Comput. Biol.* **14**, e1006617 (2018). doi:10.1371/journal.pcbi.1006617 Medline

67. A. Buckle, C. A. Brackley, S. Boyle, D. Marenduzzo, N. Gilbert, Polymer simulations of heteromorphic chromatin predict the 3D folding of complex genomic loci. *Mol. Cell* **72**, 786–797.e11 (2018). doi:10.1016/j.molcel.2018.09.016 Medline

68. C. A. Brackey, D. Marenduzzo, N. Gilbert, Mechanistic modeling of chromatin folding to understand function. *Nat. Methods* **17**, 767–775 (2020). doi:10.1038/s41592-020-0852-6 Medline

69. H. Salari, M. Di Stefano, D. Jost, Spatial organization of chromosomes leads to heterogeneous chromatin motion and drives the liquid- or gel-like dynamical behavior of chromatin. *Genome Res.* **32**, 28–43 (2022). doi:10.1101/gr.275827.121 Medline

70. D. B. Brückner, B. Zoller, dbrueckner/DynamicChromosome: initial release, Zenodo (2023); https://zenodo.org/record/7926778.

71. D. B. Brückner, H. Chen, L. Barinov, B. Zoller, T. Gregor, Trajectory data for: Stochastic motion and transcriptional dynamics of pairs of distal DNA loci on a compacted chromosome, Zenodo (2023); https://zenodo.org/record/7616203.

72. S. J. Gratz, F. P. Ukken, C. D. Rubinstein, G. Thiede, L. K. Donohue, A. M. Cummings, K. M. O'Connor-Giles, Highly specific and efficient CRISPR/Cas9-catalyzed homology-directed repair in *Drosophila*. *Genetics* **196**, 961–971 (2014). doi:10.1534/genetics.113.160713 Medline

73. K. J. T. Venken, K. L. Schulze, N. A. Haelterman, H. Pan, Y. He, M. Evans-Holm, J. W. Carlson, R. W. Levis, A. C. Spradling, R. A. Hoskins, H. J. Bellen, MiMIC: A highly versatile transposon insertion resource for engineering *Drosophila melanogaster* genes. *Nat. Methods* **8**, 737–743 (2011). doi:10.1038/nmeth.1662 Medline

74. H. Chen, Z. Xu, C. Mei, D. Yu, S. Small, A system of repressor gradients spatially organizes the boundaries of Bicoid-dependent target genes. *Cell* **149**, 618–629 (2012). doi:10.1016/j.cell.2012.03.018 Medline

75. H. Chen, T. Gregor, "Using RNA tags for multicolor live imaging of chromatin loci and transcription in *Drosophila* embryos," in *RNA Tagging: Methods and Protocols*, M. Heinlein, Ed. (Springer, 2020), pp. 373–384.

76. J. O. Dubuis, G. Tkacik, E. F. Wieschaus, T. Gregor, W. Bialek, Positional information, in bits. *Proc. Natl. Acad. Sci. U.S.A.* **110**, 16301–16308 (2013). doi:10.1073/pnas.1315642110 Medline

77. N. Otsu, A threshold selection method from gray-level histograms. *IEEE Trans. Syst. Man Cybern.* **9**, 62–66 (1979). doi:10.1109/TSMC.1979.4310076

78. L. R. Rabiner, A tutorial on hidden Markov models and selected applications in speech recognition. *Proc. IEEE* **77**, 257–286 (1989). doi:10.1109/5.18626

79. W. K. Hastings, Monte Carlo sampling methods using Markov chains and their applications. *Biometrika* **57**, 97–109 (1970). doi:10.1093/biomet/57.1.97

80. D. T. Gillespie, Stochastic simulation of chemical kinetics. *Annu. Rev. Phys. Chem.* **58**, 35–55 (2007). doi:10.1146/annurev.physchem.58.032806.104637 Medline

81. E. L. Kaplan, P. Meier, Nonparametric estimation from incomplete observations. *J. Am. Stat. Assoc.* **53**, 457–481 (1958). doi:10.1080/01621459.1958.10501452

82. B. Efron, Bootstrap methods: Another look at the jackknife. *Ann. Stat.* **7**, 1–26 (1979). doi:10.1214/aos/1176344552

83. B. Efron, R. J. Tibshirani, *An Introduction to the Bootstrap* (CRC Press, 1994).

84. C. R. Harris, K. J. Millman, S. J. van der Walt, R. Gommers, P. Virtanen, D. Cournapeau, E. Wieser, J. Taylor, S. Berg, N. J. Smith, R. Kern, M. Picus, S. Hoyer, M. H. van Kerkwijk, M. Brett, A. Haldane, J. F. Del Río, M. Wiebe, P. Peterson, P. Gérard-Marchant, K. Sheppard, T. Reddy, W. Weckesser, H. Abbasi, C. Gohlke, T. E. Oliphant, Array programming with NumPy. *Nature* **585**, 357–362 (2020). doi:10.1038/s41586-020-2649-2 Medline

85. P. Virtanen, R. Gommers, T. E. Oliphant, M. Haberland, T. Reddy, D. Cournapeau, E. Burovski, P. Peterson, W. Weckesser, J. Bright, S. J. van der Walt, M. Brett, J. Wilson, K. J. Millman, N. Mayorov, A. R. J. Nelson, E. Jones, R. Kern, E. Larson, C. J. Carey, İ. Polat, Y. Feng, E. W. Moore, J. VanderPlas, D. Laxalde, J. Perktold, R. Cimrman, I. Henriksen, E. A. Quintero, C. R. Harris, A. M. Archibald, A. H. Ribeiro, F. Pedregosa, P. van Mulbregt, A. Vijaykumar, A. P. Bardelli, A. Rothberg, A. Hilboll, A. Kloeckner, A. Scopatz, A. Lee, A. Rokem, C. N. Woods, C. Fulton, C. Masson, C. Häggström, C. Fitzgerald, D. A. Nicholson, D. R. Hagen, D. V. Pasechnik, E. Olivetti, E. Martin, E. Wieser, F. Silva, F. Lenders, F. Wilhelm, G. Young, G. A. Price, G.-L. Ingold, G. E. Allen, G. R. Lee, H. Audren, I. Probst, J. P. Dietrich, J. Silterra, J. T. Webber, J. Slavič, J. Nothman, J. Buchner, J. Kulick, J. L. Schönberger, J. V. de Miranda Cardoso, J. Reimer, J. Harrington, J. L. C. Rodríguez, J. Nunez-Iglesias, J. Kuczynski, K. Tritz, M. Thoma, M. Newville, M. Kümmerer, M. Bolingbroke, M. Tartre, M. Pak, N. J. Smith, N. Nowaczyk, N. Shebanov, O. Pavlyk, P. A. Brodtkorb, P. Lee, R. T. McGibbon, R.

Feldbauer, S. Lewis, S. Tygier, S. Sievert, S. Vigna, S. Peterson, S. More, T. Pudlik, T. Oshima, T. J. Pingel, T. P. Robitaille, T. Spura, T. R. Jones, T. Cera, T. Leslie, T. Zito, T. Krauss, U. Upadhyay, Y. O. Halchenko, Y. Vázquez-Baeza; SciPy 1.0 Contributors, SciPy 1.0: Fundamental algorithms for scientific computing in Python. *Nat. Methods* **17**, 261–272 (2020). doi:10.1038/s41592-019-0686-2 Medline

86. J. D. Hunter, Matplotlib: A 2D Graphics Environment. *Comput. Sci. Eng.* **9**, 90–95 (2007). doi:10.1109/MCSE.2007.55

Acknowledgments

We thank R. Evearers, L. Giorgetti, A. Grosberg, S. Grosse-Holz, M. Levo, L. Mirny, A. Rosa, V. Scolari, A. Spakowitz, and G. Tkacik for ~~their~~ helpful comments and discussion~~. We thank~~ K. Bystricky for introducing us to the ParB/parS system~~,~~ and F. Payre and P. Valenti for sharing the~~a~~ ParB-eGFP plasmid and the parS sequence.

Funding: This work was supported in part by the U.S. National Science Foundation, ~~through~~ the Center for the Physics of Biological Function (grant PHY-1734030), and ~~by~~ the National Institutes of Health (g~~G~~rants R01GM097275, U01DA047730, and U01DK127429). D.B.B. was supported by the NOMIS F~~f~~oundation as a ~~NOMIS F~~fellow and by an EMBO p~~P~~ostdoctoral f~~F~~ellowship (ALTF 343-2022). H.C. was supported by a~~the~~ Charles H. Revson Biomedical Science Fellowship.

Author contributions: H.C. and T.G. designed the experiments. H.C. and L.B. performed the experiments and analyzed the images~~ analysis~~. D.B.B. and B.Z. analyzed the data. D.B.B. and T.G. interpreted the data. D.B.B., B.Z., and T.G. wrote the manuscript.

Competing interests: The a~~A~~uthors declare ~~that they have~~ no competing interests.

Data and materials availability: The code and software used in this study (*70*) and the raw trajectory data (*71*) are freely available through Zenodo.

Supplementary Materials

science.org/doi/10.1126/science.adf5568

Materials and Methods

Figs. S1 to S23

Tables S1 to S8

References (*72–86*)

Movies S1 to S7

MDAR Reproducibility Checklist

View/request a protocol for this paper from *Bio-protocol*.

Submitted 29 October 2022; accepted 31 May 2023

Fig. 1. Simultaneous tracking of DNA loci and transcriptional activity in living embryos. (**A**) Typical surface view of a representative fly embryo, displaying fluorescent foci for MS2, parS, and PP7 in the corresponding blue (top), green (center), and red (bottom) channels. Top inset shows schematic with image location in the embryo; bottom inset shows a close-up. (**B**) Top: schematic of the gene cassettes used for three-color imaging. The endogenous *eve* locus (left) is tagged with MS2 stem-loops that are labeled via with blue fluorescence. A reporter with an *eve* promoter driving PP7 transcription (labeled via with red fluorescence) is integrated at a genomic separation s from the *eve* locus on the second 2nd chromosome in the *Drosophila* genome. It includes a *homie* insulator sequence allowing loop formation through *homie*–*homie* pairing, and a parS sequence that is permanently labeled with green fluorescence. Seven such constructs were generated with varying genomic separation s (triangles). Bottom: sample inter-locus distance trajectories $R(t)$ $R(t)$ for six genomic separations, with standardized y-axis limits (0, 2 μm 0, 2 μm) and x-axis limits (0, 30 min 0, 30 min), obtained following after nucleus and locus segmentation, tracking, chromatic aberration, and motion correction (see the Methods Section materials and methods, section 1). The sampling time interval is 28 s 28 s. (**C**) Trajectories of inter-locus distance R R and transcriptional activity, with inferred topological states shown by the colored top bar (blue, O_{off} O_{off}; cyan, P_{off}; P_{off}, red, P_{on}; P_{on}; see the Methods Section materials and methods, section 2). Inset: Schematic of the three topological states. (**D**) 200 examples of state trajectories sampled from a total set of $N = 579$ $N = 579$ trajectories acquired in $n = 30$ $n = 30$ embryos (genomic separation $s = 149$ kb $s = 149$ kb). Colors are as in (C). Gray trajectory parts correspond to untrackable time points.

Fig. 2. Scaling of interlocus distances and transcriptional activity across genomic separations. (**A**) Probability distributions of the inter-locus distances R R. Distributions are separated by state, with paired states pooled across genomic separations, and individual distributions are shown for the open state. (**B**) Average inter-locus distances $\langle R \rangle$ $\langle R \rangle$ for each of the three transcriptional states. Blue dashed line indicates a linear best fit to the O_{off} O_{off} data for the range of genomic separations 58 to 190 kb, with exponent $1/d = 0.31 \pm 0.07$ $1/d = 0.31 \pm 0.07$. Dashed cyan and red lines are average values of the interlocus distances of the P_{off} P_{off} and P_{on} P_{on} states, respectively, with shaded areas indicating error of the mean SEM. Solid dark green and red lines indicate predictions for ideal and crumpled polymers, respectively. (**C**) Survival curves $S(t)$ $S(t)$ of the transcriptionally active state P_{on} P_{on}, giving the probability that transcription remains active after time t t. Orange curve: data for no-*homie* constructs ($s = 58$ $s = 58$ kb). Curves were estimated using the Kaplan-Meier estimator, which accounts for censoring, which that occurs if the trajectory begins or ends in the transcriptionally active state (*81*). Shaded areas show 95% confidence intervals (see the Methods Section materials and methods, section 2.4). (**D**) Median lifetime of the transcriptionally active state P_{on} P_{on} as a function of genomic separation, using the Kaplan-Meier estimator (dots) and a maximum-likelihood estimator assuming exponential decay of the survival curves (triangles) (see the Methods Section materials and methods, section 2.4). (**E**) Probability of the paired on and off states conditioned on the system being in one of these two paired configurations. (**F**) Overall probability of the paired configurations P_{off} P_{off} and P_{on} P_{on} as a function of genomic separation. Gray line is the best fit with exponent 0.9 ± 0.2 0.9 ± 0.2. Green and dark red lines

indicate predicted exponents for the contact probabilities of the ideal and crumpled chain polymer models, respectively.

Fig. 3. Dynamics of DNA locus search and single-locus fluctuations. (**A**) Single-cell inter-locus distance trajectories for the three topological states (s = 149 ~~$s = 149$~~ kb). For each state, 80 trajectories are shown, with one sample trajectory highlighted in bold. (**B**) Distance distributions (bar histogram) of the highlighted trajectory in ~~panel~~ (C) compared ~~to~~ with the ensemble distribution obtained by averaging over all cells (line). (**C**) Single-cell inter-locus distance distributions (thin lines) of all trajectories ~~in panel (C)~~ for the three states compared ~~to~~ with ensemble distributions in bold (s = 149 ~~$s = 149$~~ kb). Distributions are smoothed using Gaussian kernel density estimation with a width of 100 nm ~~100 nm~~. Only trajectories with at least ~~ten~~ 10 time points are included to ensure sufficient statistics for comparison. (**D**) Single-locus MSDs for all genomic separations (color code corresponds to Fig. 2A). Single-locus MSDs ~~are~~ were calculated by estimating 3D MSDs from motion-corrected trajectories in the x-y ~~xy~~-plane of the system (see the ~~Methods Section~~materials and methods, section 3). Open data points correspond to a shorter imaging time interval Δt = 5.4 s ~~$\Delta t = 5.4$ s~~ (s = 149 ~~$s = 149$~~ kb). (**E**) Single-locus MSDs comparing enhancer (blue) and promoter (green) fluctuations (s = 149 ~~$s = 149$~~ kb). (**F**) Single-locus MSDs comparing fluctuations in the three states (s = 149 ~~$s = 149$~~ kb).

Fig. 4. Joint dynamics of DNA locus pairs. ~~(Continued on the following page.)~~ (**A**) Ideal chain Rouse prediction of the two-locus MSD $M_2(t) = 2\Gamma t^{1/2}(1 - e^{-\tau/\pi t}) + 2J\ \mathrm{erfc}[(\tau/\pi t)^{1/2}]$ ~~$M_2(t) = 2\Gamma t^{1/2}\left(1 - e^{-\tau/\pi t}\right) + 2J\ \mathrm{erfc}\left[(\tau/\pi t)^{1/2}\right]$~~ (*26*) (graey line), using best fit values Γ, J, β = 1/2, and $\tau = (J/\Gamma)^2$ ~~$\Gamma, J, \beta = 1/2$, and $\tau = (J/\Gamma)^2$~~, compared ~~to~~ with experiment (s = 595 ~~$s = 595$~~ kb). Green and red lines give expected scaling t^{β} ~~t^{β}~~ for $t \ll \tau$ ~~$t \ll \tau$~~ for the generalized Rouse model for ideal and crumpled chains, respectively (see the ~~Methods Section~~materials and methods, section 5). (**B**) All experimental two-locus MSDs with relaxation times (dashed lines) and expected asymptotes $2\langle R^2\rangle$ ~~$2\langle R^2\rangle$~~ (solid lines; color code corresponds to Fig. 2A). (**C**) Scaling of the diffusion coefficients Γ ~~Γ~~ from two-locus MSD fits (black dots), compared ~~to~~ with single-locus diffusion coefficients obtained from single-locus MSDs (Fig. 3, F to H). Dashed line is the best fit to two-locus diffusivity with exponent 0.27 ± 0.03 ~~0.27 ± 0.03~~ (s = 58 to 595 ~~$s = 58 - 595$~~ kb); solid lines are the average value of single locus diffusivities; shaded area shows ~~error (std.~~ SE calculated from total variance across separations~~)~~. (**D**) Two-locus autocorrelation function (ACF) $C_2(t) = \langle \mathbf{R}(t_0)\cdot\mathbf{R}(t_0+t)\rangle_{t_0} = \langle R^2\rangle - M_2(t)/2$ (graey) compared with~~to~~ data (s = 149 ~~$s = 149$~~ kb). Green and red curves indicate the power-law exponent $\lambda = 2(1 - d)/(2 + d)$ ~~$\lambda = 2(1-d)/(2+d)$~~ of the correlation function $C_2(t) \sim t^{\lambda}$ ~~$C_2(t) \sim t^{\lambda}$~~ for ideal and crumpled chains for $t \gg \tau$ ~~$t \gg \tau$~~, respectively (*39*). (**E**) Collapsed correlations $C_2 \sim C_2(ts^{-\gamma})/\langle R^2\rangle$ ~~$C_2 \sim C_2\left(ts^{-\gamma}\right)/\langle R^2\rangle$~~ with γ = 0.7 ~~$\gamma = 0.7$~~. Inset: ~~*Inset:*~~ raw correlations $C_2(t)$ ~~$C_2(t)$~~ for varying genomic separation. Open data points correspond to data obtained with a higher sampling rate. (**F**) Scaling of inferred relaxation times compared ~~to~~ with predicted ideal and crumpled chain exponents. Graey line is the best fit with exponent γ = 0.7 ± 0.2 ~~$\gamma = 0.7 \pm 0.2$~~. (**G**) Predicted velocity cross-correlation functions $C_{vv}^{(\delta)}(t) = \langle \mathbf{v}_i^{(\delta)}(t_0)\cdot\mathbf{v}_j^{(\delta)}(t_0+t)\rangle_{t_0}$ for increasing values of the dimensionless ratio δ/τ ~~δ/τ~~ (*55*). Velocities are calculated on a time interval δ ~~δ~~ as $\mathbf{v}^{(\delta)}(t)$ =

[**x**(*t* + δ) – **x**(*t*)]/δ. $\mathbf{v}^{(\delta)}(t) = (\mathbf{x}(t+\delta) - \mathbf{x}(t))/\delta$. (**H**) Scaling of the zero-time velocity cross-correlation intercept normalized by the zero-time auto-correlation, $C_{vv}^{(\delta)}(0)/C_{v}^{(\delta)}(0)$, for the O_{off} (O_{off}) (blue) and P_{on} (P_{on}) (red) states; δ = 300 s (δ = 300 s). Green line is the: prediction based on ideal chain Rouse scaling of the relaxation times (γ = 2 (γ = 2)) with an intercept determined based on the 58-58 kb data point; graey line is the: parameter-free prediction using the inferred anomalous relaxation time scaling (γ ≈ 0.7 (γ ≈ 0.7)) (see the Methods Sectionmaterials and methods, section 4.3); dashed red line: is the average correlation in the P_{on} (P_{on}) state.

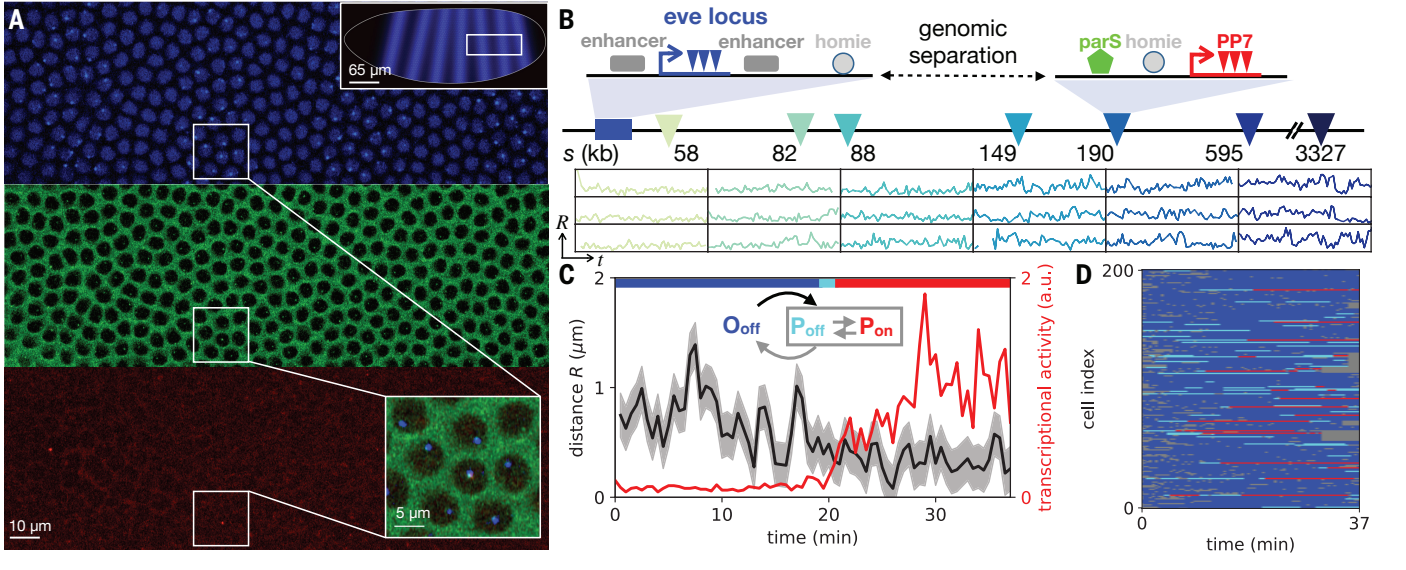
A
65 µm
10 µm
5 µm
B
eve locus
enhancer
enhancer
homie
genomic separation
parS
homie
PP7
s (kb)
58
82
88
149
190
595
3327
R
t
C
2
1
0
distance R (µm)
Ooff
Poff
Pon
2
0
transcriptional activity (a.u.)
0
10
20
30
time (min)
D
200
0
cell index
0
37
time (min)

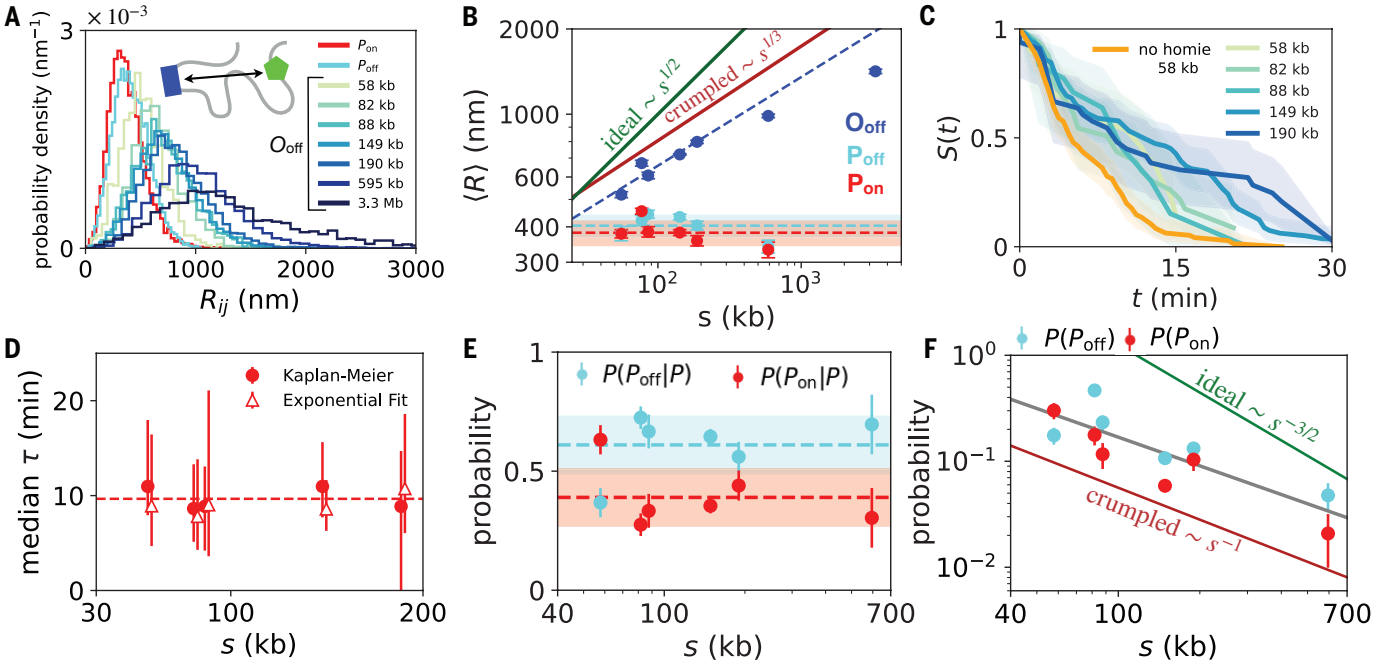
A
B
C
D
E
F
probability density (nm⁻¹)
× 10⁻³
R_{ij} (nm)
P_{on}
P_{off}
58 kb
82 kb
88 kb
149 kb
190 kb
595 kb
3.3 Mb
O_{off}
⟨R⟩ (nm)
ideal ~ s^1/2
crumpled ~ s^1/3
Off
Poff
Pon
s (kb)
S(t)
no homie
58 kb
t (min)
median τ (min)
Kaplan-Meier
Exponential Fit
probability
P(Poff|P)
P(Pon|P)
P(Poff)
P(Pon)
ideal ~ s^−3/2
crumpled ~ s^−1

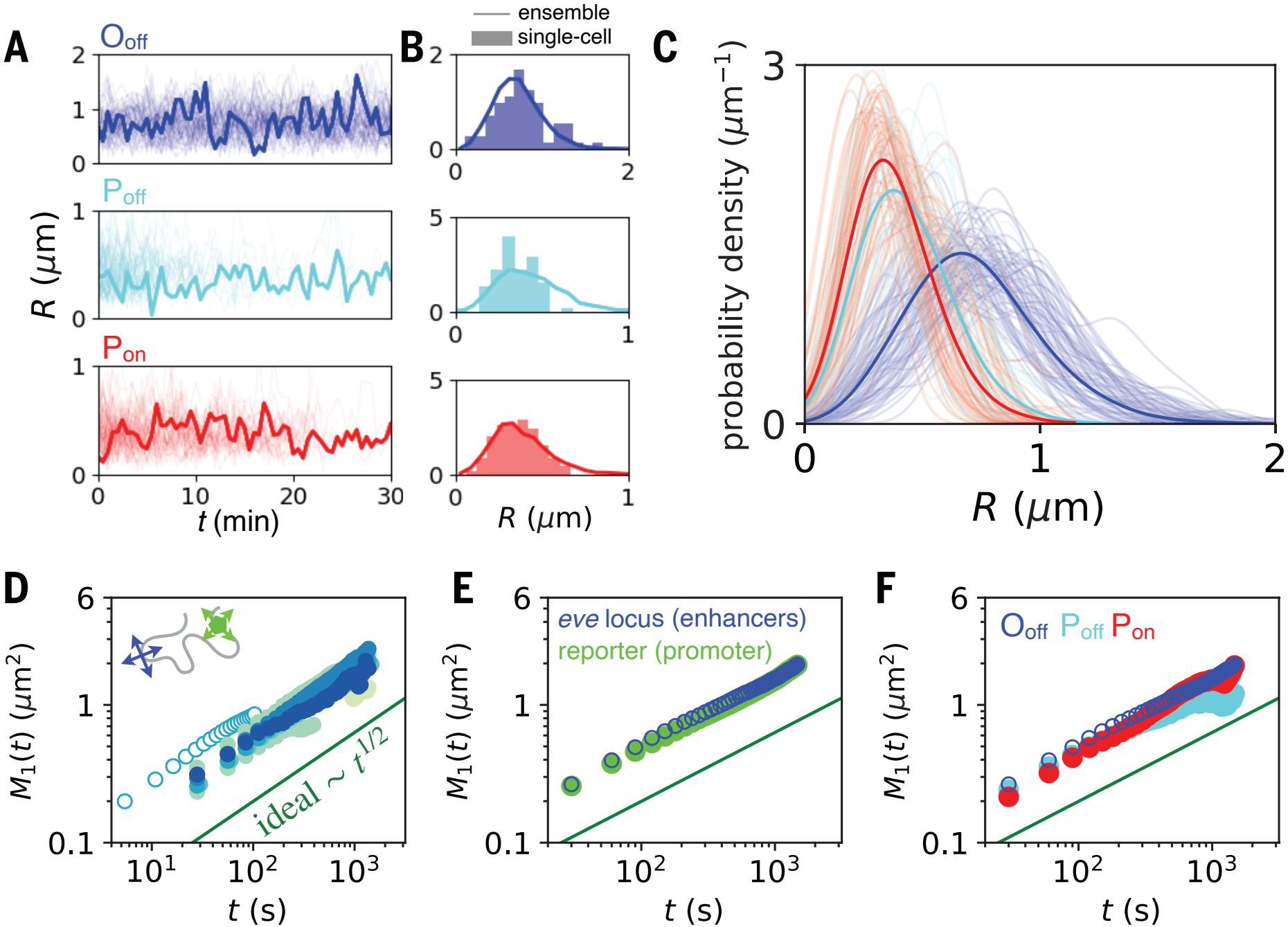
A
B
C
D
E
F
O_{off}
P_{off}
P_{on}
R (μm)
t (min)
ensemble
single-cell
probability density (μm^{-1})
R (μm)
$M_1(t)$ (μm^2)
t (s)
ideal ~ $t^{1/2}$
eve locus (enhancers)
reporter (promoter)
O_{off} P_{off} P_{on}

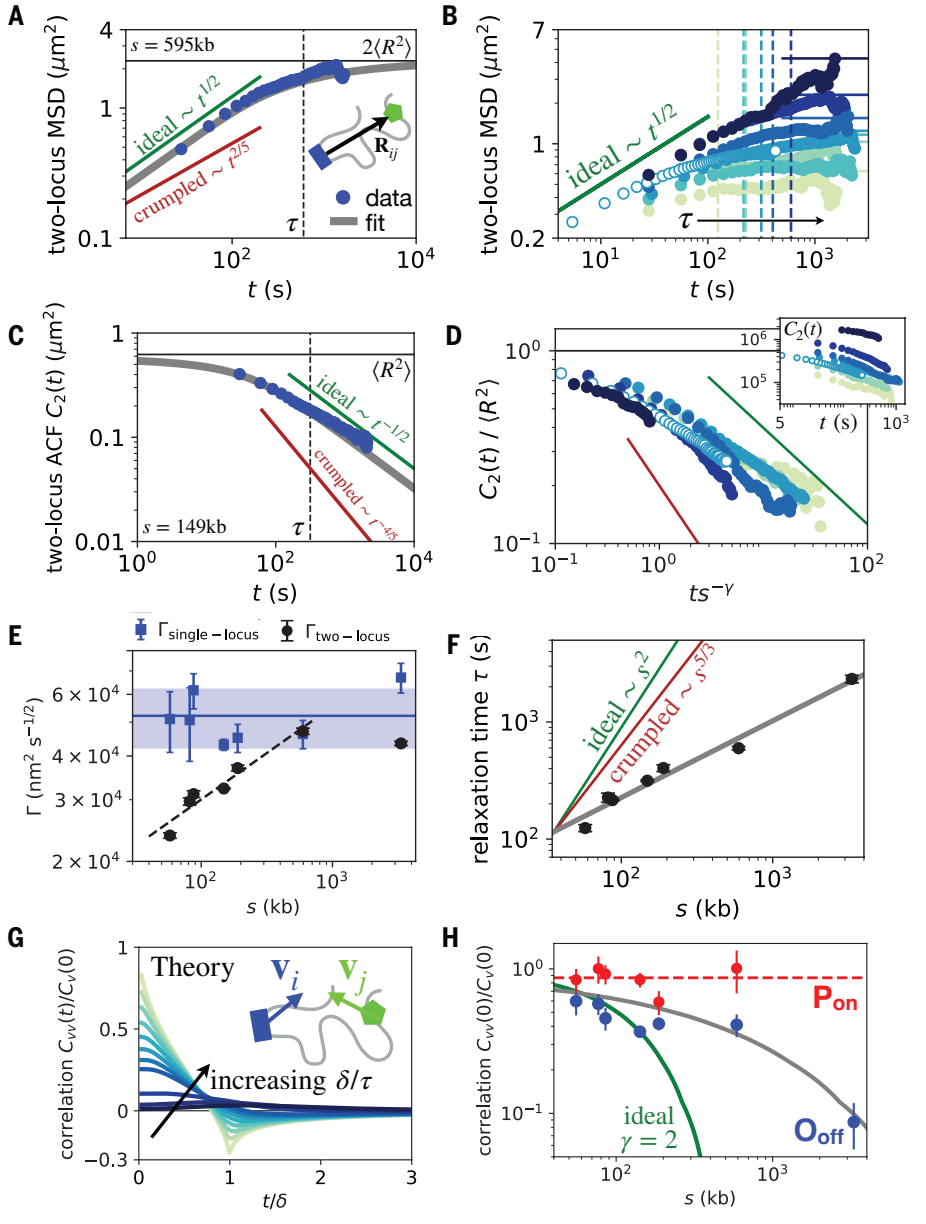
A
two-locus MSD (μm^2)
s = 595kb
$2\langle R^2\rangle$
ideal ~ $t^{1/2}$
crumpled ~ $t^{2/5}$
$\mathbf{R}_{ij}$
data
fit
τ
t (s)
B
two-locus MSD (μm^2)
ideal ~ $t^{1/2}$
τ
t (s)
C
two-locus ACF $C_2(t)$ (μm^2)
$\langle R^2\rangle$
ideal ~ $t^{-1/2}$
crumpled ~ $t^{-4/5}$
s = 149kb
τ
t (s)
D
$C_2(t) / \langle R^2\rangle$
$C_2(t)$
t (s)
$ts^{-\gamma}$
E
$\Gamma_{single-locus}$
$\Gamma_{two-locus}$
Γ (nm^2 s$^{-1/2}$)
s (kb)
F
relaxation time τ (s)
ideal ~ s^2
crumpled ~ $s^{5/3}$
s (kb)
G
correlation $C_{vv}(t)/C_v(0)$
Theory
$\mathbf{v}_i$
$\mathbf{v}_j$
increasing δ/τ
t/δ
H
correlation $C_{vv}(0)/C_v(0)$
$\mathbf{P}_{on}$
$\mathbf{O}_{off}$
ideal
$\gamma = 2$
s (kb)